Three novel high-resolution nonlinear methods for fast signal processing

Dž. Belkić[a] and P. A. Dando
Department of Chemistry, University of Southern California, Los Angeles, California 90089-0482 and Department of Medical Radiation Physics, Karolinska Institute, P.O. Box 260, S-17176 Stockholm, Sweden

J. Main
Institut für Theoretische Physik und Synergetik, Universität Stuttgart, D-70550 Stuttgart, Germany

H. S. Taylor[b]
Department of Chemistry, University of Southern California, Los Angeles, California 90089-0482

(Received 6 June 2000; accepted 26 July 2000)

Three novel nonlinear parameter estimators are devised and implemented for accurate and fast processing of experimentally measured or theoretically generated time signals of arbitrary length. The new techniques can also be used as powerful tools for diagonalization of large matrices that are customarily encountered in quantum chemistry and elsewhere. The key to the success and the common denominator of the proposed methods is a considerably reduced dimensionality of the original data matrix. This is achieved in a preprocessing stage called beamspace windowing or band-limited decimation. The methods are decimated signal diagonalization (DSD), decimated linear predictor (DLP), and decimated Padé approximant (DPA). Their mutual equivalence is shown for the signals that are modeled by a linear combination of time-dependent damped exponentials with stationary amplitudes. The ability to obtain all the peak parameters first and construct the required spectra afterwards enables the present methods to phase correct the absorption mode. Additionally, a new noise reduction technique, based upon the stabilization method from resonance scattering theory, is proposed. The results obtained using both synthesized and experimental time signals show that DSD/DLP/DPA exhibit an enhanced resolution power relative to the standard fast Fourier transform. Of the three methods, DPA is found to be the most efficient computationally. © *2000 American Institute of Physics.* [S0021-9606(00)00440-2]

I. INTRODUCTION

A novel method called decimated signal diagonalization (DSD) has recently been suggested in Ref. 1 to solve a class of generalized eigenvalue problems with large matrices whose elements are autocorrelation functions stemming from time propagated wave packets. Successful performance of DSD was demonstrated with a long noiseless synthesized signal having the known peak parameters as well as with a theoretically calculated energy spectrum of SO_2 for some ~ 5000 bound vibrational levels below $25\,000\,\mathrm{cm}^{-1}$. Moreover, in Ref. 1 DSD was shown to agree perfectly with the results of Ref. 2 obtained using the filter diagonalization (FD) method.[3,4] Subsequently in Refs. 5 and 6, DSD was also extended to signal processing. This was made possible by the well-known equivalence between the autocorrelation functions and exponentially damped time signals associated with the Lorentzian-type spectra.[3,4] Such signals are often encountered in many experiments performed with, e.g., ion cyclotron resonance (ICR) and Nuclear magnetic resonance (NMR) techniques.[7,8] The results reported in Refs. 5 and 6 for simulated and measured signals demonstrate the superior capability of DSD to resolve the spectral features that are practically inaccessible to fast Fourier transform (FFT) at shorter acquisition times. This conclusion usually holds true not only for nearly noise free signals, but also for signals that are embedded in a considerable noise background. In FFT all the frequencies are fixed and restricted to the set of Fourier grid points that are predetermined by the total acquisition time. By contrast, DSD considers both the complex frequencies and amplitudes as the fitting parameters. This enables higher resolution in DSD whose estimated frequencies could be much closer to each other than the usual Fourier grid spacings.[5,6]

In its processing stage, DSD effectively uses the operative part of the discrete version of FD,[4] which constructs matrices of a generalized eigenvalue problem directly from digitized signal points. Diagonalization first supplies the peak parameters, e.g., the positions, heights, widths, and phases, so that Lorentzian spectra can subsequently be computed in any desired mode (absorption, magnitude, power, etc). As with FD, the key to the success of DSD is in windowing, the purpose of which is a sizable reduction of the original large dimensionality of the data matrix to be diagonalized. Severe numerical instabilities always plague diagonalization of large matrices and even the Cholesky, Householder or singular value decomposition (SVD) are known to be unable to bring the mathematical ill-conditioning of the problem under reasonable control. This, together with the emergence of extraneous peaks, is due to the fact that the matrix dimension, which equals half the signal length N, is much larger than the matrix rank, i.e., the number of spectral

[a]Electronic mail: belkic@radfys.ks.se
[b]Electronic mail: taylor@cheml.usc.edu

 © 2000 American Institute of Physics

Lorentzians. From the numerical viewpoint, DSD shares a feature of FD that necessitates the calculation of both eigenfrequencies *and* eigenfunctions. These are provided by initially diagonalizing the overlap matrix over the Krylov (DSD) or Fourier–Krylov (FD) basis functions and subsequently solving the resulting generalized eigenvalue problem for the time evolution operator.

Windowing is accomplished in DSD while preprocessing the time signal and, hence, this stage of the analysis is completely dissociated from the subsequent diagonalization for which the Krylov basis functions suffice.[1,5,6] This so-called beamspace windowing, which is also known as band-limited decimation, has previously been used in other research fields, e.g., radar problems,[9] etc. The signals that are ''beamspaced in DSD'' could equally well be subjected to any other estimators as emphasized in Ref. 1 and illustrated in Ref. 5. This is in contrast to the windowing used in FD which takes place *during* the diagonalization step in the course of setting up the Fourier–Krylov basis functions[3,4] and, as such, cannot be used with any other processing method.

The present paper explores several possibilities offered by the reduced dimensionality of beamspaced signals. Such shorter signals could potentially revive the interest in a number of other signal processing methods whose widespread applications have thus far been hampered by large data matrices. Here, in addition to a further usage of DSD, we shall focus our attention on two such techniques known as the linear predictor (LP) and Padé approximant (PA). When employing band-limited decimated signals, the latter two methods will be termed decimated linear predictor (DLP) and decimated Padé approximant (DPA), in accordance with Ref. 5, where they have been applied to the problem of the periodic orbit quantization.

The LP is well known in signal processing.[10] Here, modeling time signals with sums of damped exponentials with constant amplitudes proceeds through solving two systems of linear equations, one for the LP coefficients and the other for the amplitudes. The latter step can only be undertaken when rooting of the characteristic polynomial, constructed from the LP coefficients, has been accomplished. Any rooting is a nonlinear problem and, therefore, LP is an inherently nonlinear signal processor. The previous applications of LP have been limited to relatively short signals for the obvious reason of ill-conditioning of large matrices. This chief obstacle can be circumvented successfully by subjecting the band-limited decimated signal to LP, rather than analyzing the original one, at no loss of information in the selected frequency interval. It is in this way that DLP emerges. Its usefulness has already been demonstrated in Ref. 5 and will be further explored in this paper.

The PA is also a well-known technique which has frequently been used to accelerate convergence of slowly convergent series.[11,12] In signal processing it was used before under the name autoregressive moving average.[10] Additionally, PA is successful in analytically continuing purely divergent series or sequences with, e.g., exponentially growing terms[13] or even those with zero radius of convergence.[14] In short, PA maps a given power series into a rational function expressed as a quotient of two polynomials. In signal processing, the discrete Fourier transform (DFT) is a polynomial in a complex exponential (a harmonic) taken at the Fourier frequencies. Increasing its order, such a polynomial exhibits a rather slow convergence rate which is equal to the inverse of the signal length. This can be significantly accelerated by using PA for relatively short signals. For long signals, construction of the numerator and denominator polynomials in PA becomes numerically intractable. It is here that we need band-limited decimated signals to create relatively short and manageable DFTs that are subsequently subjected to PA, which then acquires the acronym DPA, as indicated previously. This new method in signal processing is also a parametric estimator. Here, the frequencies sought are related simply to the roots of the denominator polynomial. Moreover, the corresponding magnitudes are obtained without any additional effort from an analytical formula for the residues of the Padé quotient of the polynomials.

For the Lorentzian spectra, DSD, DLP, and DPA are shown to be mathematically equivalent to each other despite their different numerical algorithms. The demonstration relies upon the fact that the given eigenvalue problem is basically equivalent to its secular equation. The latter is the characteristic polynomial which is identical to the denominator polynomial of DPA as well as to the DLP polynomial yielding the peak frequencies.

Crucially, given the signal length, DSD, DLP, and DPA yield a higher resolution than available in FFT. This is usually accomplished with an improved convergence rate, which often implies a considerably shorter acquisition time than that required by FFT. This property might be used advantageously in conventional ICR and NMR experiments where the longer signals required by FFT practically always invoke more noise. The present methods effectively attain the necessary convergence before exhausting the full length of the signal. These statements are supported in sec. III by the evidence presented for several experimental ''noisy'' signals as well as a synthesized signal comprised of a number of completely known harmonics. Conclusions are given in Sec. IV.

II. THEORY

In this section we shall describe the DSD, DLP and DPA methods as the new parameter estimators. This will be done using the generic concept called ''band-limited decimation'' [1] or equivalently ''beamspace windowing,'' [6] which has been previously known in the engineering literature as ''beamspace.'' [9] These alternative names will be used interchangeably whenever referring to this specific windowing, which is different than that implemented in FD.[3,4] Further we will show under which conditions these three signal processing techniques become mathematically equivalent to each other in spite of rather different numerical computations. The present study will be restricted to those time signals that are sums of damped exponentials with complex frequencies and amplitudes, $\{\omega_k, d_k\}$. Moreover, we shall be concerned primarily with the local spectral analysis carried out in a window of interest, $[\omega_{\min}, \omega_{\max}]$.

A. Beamspace windowing

Beamspace windowing is a conceptually simple method that enables the construction of a shortened signal which is amenable to processing by DSD, DLP and DPA. We start with a digitized time signal $\{c_n\}(0\leqslant n\leqslant N-1)$ which consists of N points, equidistantly sampled with the rate τ and having a total bandwidth of $2\pi/\tau$. To initialize windowing, $\{c_n\}$ is subjected to a discrete Fourier transform using the efficient FFT algorithm to obtain the Fourier spectrum,

$$F_k=\sum_{n=0}^{N-1} c_n e^{2\pi ikn/N}, \quad (k=0,\ldots,N-1), \tag{1}$$

which is accurate only at the Fourier grid points, k, corresponding to the frequencies $\overline{\omega}_k=2\pi k/(N\tau)$. In general, the FFT of Eq. (1) yields only a low-resolution spectrum as the number of signal points, N, will be insufficient for the FFT to resolve dense eigenfrequencies. We assume, however, that N is sufficiently large for harmonic inversion to be possible, i.e., $N\geqslant 2K'$ where K' is the total number of frequency components contained in the signal.

Next, the frequency window of interest, $[\overline{\omega}_{k_{\min}},\overline{\omega}_{k_{\max}}]$, is chosen. In order to diminish the ill-conditioning of the subsequent processing, the number of Fourier grid points, $N_D=k_{\max}-k_{\min}+1$, contained in the window should not exceed more than about 200. The N_D elements, F_k, of the low resolution Fourier spectrum located within the window are then selected and shifted to relocate them symmetrically about the frequency origin, $\omega=0$. In other words, the central frequency of the window, $\omega_0=2\pi k_0/(N\tau)$ where $k_0=(k_{\max}+k_{\min})/2$, is subtracted from every frequency ω belonging to the actual window. In this way, the band-limited FFT spectrum, $\{F_k^{\rm bld}\}$ $(0\leqslant k\leqslant N_D-1)$ is created. Specifically, we have $F^{\rm bld}_{k-k_0}=F_k$ for $k_{\min}\leqslant k\leqslant k_{\max}$ with the periodicity of the FFT used to identify $F_j^{\rm bld}=F^{\rm bld}_{N_D+j}$ when $j<0$. The result is a spectrum that is centered at $\omega=0$ with a bandwidth of $2\pi N_D/(N\tau)$.

Finally, an inverse FFT is applied to $\{F_k^{\rm bld}\}$ to obtain the so-called ''band-limited decimated'' (bld) signal $\{c_n^{\rm bld}\}$ $(0\leqslant n\leqslant N_D-1)$ of shorter length N_D and valid for the window of interest. The new bandwidth is reduced $M=N/N_D$ times from that of the original signal. Hence the ''dwell'' time of the band-limited decimated signal is now $\tau_D=M\tau$ giving the same total acquisition time as used for c_n, i.e., $T=N\tau=N_D\tau_D$. Hence the problem has been reduced to one of signal processing a significantly shortened or ''decimated'' effective signal.

In order to scan the whole bandwidth of the original signal $[-\pi/\tau,+\pi/\tau]$, we must form the Fourier spectra $\{F_k^{\rm bld}\}$ and the resulting band-limited decimated signal $\{c_n^{\rm bld}\}$ separately for each of M windows. Note, however, that the first FFT of the original signal of length N is common to each of the M windows and hence need be performed only once.

In any of the windows, $[\overline{\omega}_{k_{\min}},\overline{\omega}_{k_{\max}}]$, the resulting FFT spectra $\{F_k^{\rm bld}\}$ created from $\{c_n^{\rm bld}\}$ are, by construction, identical (apart from the shift to $\omega=0$) to the corresponding Fourier spectra $\{F_k\}$ based solely upon $\{c_n\}$. This establishes the key feature of the procedure which is the preservation of the informational content in each of the M individual windows. We emphasize this crucial feature of the *band-limited decimation* to avoid any potential confusion with a *straightforward decimation* which always leads to a loss of information.

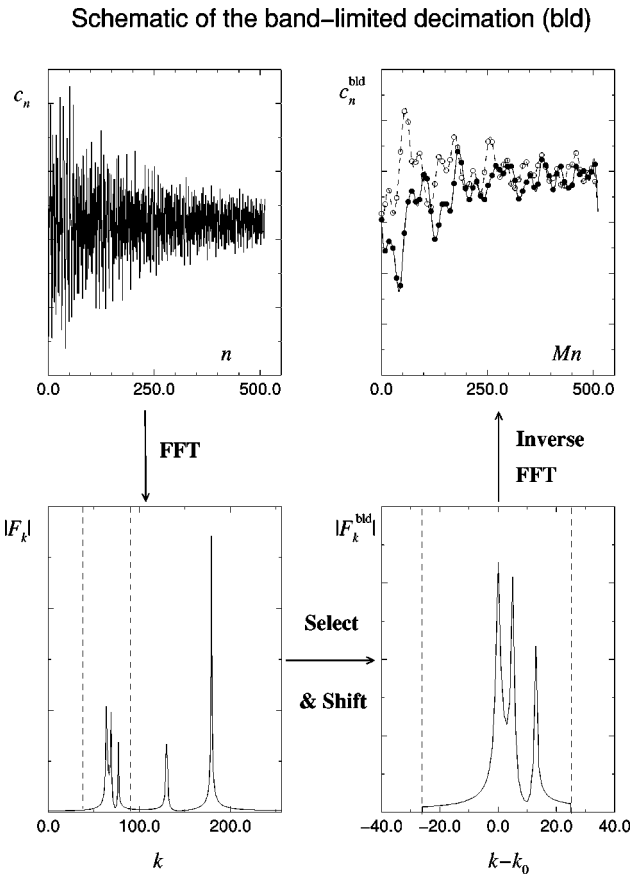

FIG. 1. Schematic of the band-limited decimation process. The original signal shown in the upper left-hand panel is first subjected to the FFT, yielding the low resolution spectrum plotted in the lower left-hand panel. A window, indicated by the dashed lines, is chosen. The values of the F_k elements outside the window are set to zero, while the remaining F_k elements within window are shifted in frequency so that the window is symmetric about $\omega=0$ (the bottom right-hand panel). An inverse FFT is then applied, yielding the real and imaginary parts of the band-limited decimated signal points, $c_n^{\rm bld}$, denoted by the full and open circles, respectively.

In summary, implementation of the described ''band-limited decimation'' (bld) proceeds through the following algorithm:

(1) Obtain the whole FFT spectrum, as an array $\{F_k\}$ of length N, from the original signal $\{c_n\}$.
(2) Select the window of interest $[\overline{\omega}_{k_{\min}},\overline{\omega}_{k_{\max}}]$ spanning a total of $N_D=k_{\max}-k_{\min}+1$ Fourier grid points.
(3) Create the band-limited FFT spectrum, $\{F_k^{\rm bld}\}$, of length N_D by selecting those F_k that lie within the window and simultaneously shifting by the central frequency, $\omega_0=2\pi k_0/(N\tau)$ where $k_0=(k_{\max}+k_{\min})/2$, to obtain a symmetrical redistribution around the origin, $\omega=0$.
(4) Construct the generally complex-valued band-limited decimated signal, $\{c_n^{\rm bld}\}$, of length N_D by subjecting $\{F_k^{\rm bld}\}$ from step 3 to the inverse FFT.

The key steps 1–4 are illustrated in Fig. 1 using a synthesized signal c_n with the known peak parameters listed in Ref. 7.

In our numerical implementation of band-limited decimation, we explicitly use the robust numerical routines for FFT and inverse FFT in steps 1 and 4 to take full advantage of the quasi-linear scaling with the signal length, $N \log_2 N$. Note, however, that the above-outlined prescription 1–4 also permits a straightforward derivation of the following analytical formula:

$$c_n^{\mathrm{bld}} = \frac{1}{N} \sum_{n'=0}^{N-1} c_{n'} e^{2\pi i n' k_0 / N} \frac{\sin(\pi N_D [n/N_D - n'/N])}{\sin(\pi [n/N_D - n'/N])}, \tag{2}$$

with $0 \leqslant n \leqslant N_D - 1$.

B. Decimated signal diagonalization

Among our three processing methods, DSD will be outlined first. Just like FD, the technique of DSD is strictly limited to the signals given as sums of damped exponentials built from complex frequencies and amplitudes, $\{\omega_k, d_k\}$. Of course, the real parts of the fitting parameters ω_k's should belong to the selected window $[\omega_{\min}, \omega_{\max}]$. We then model the band-limited decimated signal c_n^{bld} as

$$c_n^{\mathrm{bld}} = \sum_{k=1}^{K} d_k e^{-i\omega_k n \tau_D}, \quad \mathrm{Im}(\omega_k) < 0, \tag{3}$$

where the condition $\mathrm{Im}(\omega_k) < 0$ selects only the physical harmonics with decaying exponentials as the time increases. Here K is the so-called local spectral rank which is equal to the number of Lorentzians generated by Eq. (3) in the corresponding spectrum. According to Refs. 1, 3, and 4, the autocorrelation function $C_n^{\mathrm{bld}} \equiv (\Phi_0 | \exp[-i\hat{\Omega} n \tau_D] \Phi_0)$ is equivalent to the band-limited decimated signal,

$$c_n^{\mathrm{bld}} = (\Phi_0 | \exp[-i\hat{\Omega} n \tau_D] \Phi_0). \tag{4}$$

This is because insertion of the closure relation for the spectrum of the time evolution operator $U(\tau_D) = \exp(-i\hat{\Omega}\tau_D)$ into C_n^{bld} with a specific identification of d_k, leads directly to the right-hand side of Eq. (3), so that $c_n^{\mathrm{bld}} = C_n^{\mathrm{bld}}$.[3,4] Such a circumstance obviates the necessity for an explicit nonlinear fit in Eq. (3). Instead we use linear algebra to set up and solve the following equivalent generalized eigenvalue problem:

$$\mathbf{U}\mathbf{B}_k = u_k \mathbf{S}\mathbf{B}_k. \tag{5}$$

Here, the column matrix $\mathbf{B}_k$ has the elements $\{B_{nk}\}$, where B_{nk} is the kth eigenvector of $\mathbf{U}$ corresponding to the eigenvalue $u_k = e^{-i\omega_k \tau_D}$. Note that there is no need for either the operator $\hat{\Omega}$ in $U(\tau_D)$ or the initial state Φ_0 in C_n^{bld} to be given or known explicitly. The inner or scalar product in DSD is of the symmetric nature, i.e., without the complex conjugation of the bra vector $(\cdot|$ such that $(\chi|\psi) = (\psi|\chi)$. We diagonalize matrix $\mathbf{U}$ using the Krylov basis set $\{\Phi_n\}$ with the functions $\Phi_n = U^n(\tau_D)\Phi_0$ that produce the following matrix elements:[1]

$$U_{nm} = c_{n+m+1}^{\mathrm{bld}}, \quad S_{nm} = c_{n+m}^{\mathrm{bld}}. \tag{6}$$

Both U_{nm} and S_{nm} are expressed solely in terms of the signal points $\{c_n^{\mathrm{bld}}\}$ making obvious that the explicit knowledge of the pair $\{\Phi_0, \hat{\Omega}\}$ is not needed, as alluded to above. Relations similar to Eq. (6) have been encountered previously in FD,[3,4] where the original signal c_n replaces c_n^{bld}. Another interpretation of Eq. (6) is that DSD can equally well be applied to measured and/or computed signals as long as they obey Eq. (3). Having the matrix elements U_{nm} and S_{nm} at hand, DSD diagonalizes Eq. (5) to extract all the peak parameters $\{\omega_k, d_k\}$ in the chosen window $[\omega_{\min}, \omega_{\max}]$. These parameters enable one to readily construct a *local* spectrum in any desired mode, e.g. magnitude $|F(\omega)|$, power $|F(\omega)|^2$ or absorption $A(\omega)$. This final step is carried out at *any* real frequency ω from the studied window via a linear combination of complex Lorentzians, such as

$$F(\omega) = -i \sum_{k=1}^{K} \frac{d_k}{\omega - \omega_0 - \omega_k}. \tag{7}$$

Note that the real central frequency ω_0 of the window $[\omega_{\min}, \omega_{\max}]$ is explicitly added to every complex resonance ω_k. This is necessary to compensate for the shift to the origin $\omega = 0$ of the band-limited Fourier spectrum used in generating the set $\{c_n^{\mathrm{bld}}\}$. One of the possible ways to obtain an absorption spectrum, $A(\omega) \geqslant 0$, which is always positive definite for any real values of ω, has been suggested recently in Ref. 6 as

$$A(\omega) = -\sum_{k=1}^{K} |d_k| \frac{\mathrm{Im}(\omega_k)}{[\omega - \omega_0 - \mathrm{Re}(\omega_k)]^2 + [\mathrm{Im}(\omega_k)]^2}. \tag{8}$$

This absorption mode does not contain any interference effects, since the signal phase $\mathrm{Arg}(d_k)$ in $|d_k| = |d_k e^{i\mathrm{Arg}(d_k)}|$ has been intentionally omitted from Eq. (8). In general, diagonalization will produce not only the physical, $\mathrm{Im}(\omega_k) < 0$, but also the spurious, $\mathrm{Im}(\omega_k) > 0$, eigenfrequencies. The latter ones could be reflected according to the prescription $\mathrm{Im}(\omega_k) \rightarrow -|\mathrm{Im}(\omega_k)|$ as done previously in Refs. 4 and 6. To extract all the magnitudes $\{d_k\}$, DSD computes the set of the eigenvectors $\{B_{nk}\}$ which are normalized with respect to the overlap matrix $\mathbf{S}$ and employs the formula[1]

$$d_k = \left(\sum_{n=0}^{[N_D/2]} B_{nk} c_n^{\mathrm{bld}} \right)^2, \tag{9}$$

which follows from a derivation similar to that established in FD.[3,4] When using DSD to analyze noiseless signals with known parameters, Eq. (9) is found to give excellent results for the d_k's, while for FD an averaging procedure is needed[4] to achieve the same level of accuracy.

Of course, whenever needed the sequence of steps described above can be repeated M times to cover the whole Nyquist interval, as already anticipated. When proceeding along these lines, there should be no restrictions to keep the same signal length N_D for every sub-window. Some artifacts can occur in the process of ''gluing'' together the adjacent frequency intervals due to a sharp rectangular window in ''beamspacing.'' This leads to phase distortions which could somewhat deteriorate the shape of the spectrum at the edges of the windows particularly when analyzing windows that

contain a small number of Fourier grid points (i.e., small N_D). We adopt the simple procedure of Ref. 6, which allows a considerable overlap of the neighboring windows so that the narrow edges of every local spectra can be omitted. Note that the first FFT in the band-limited decimation is common to the processing of all individual windows from the Nyquist interval.

Beamspace windowing enables the passage from the original $N/2\times N/2$ matrix $\mathbf{U}$ to one of size $N_D/2\times N_D/2$ whose dimension is M times smaller. Such an achievement reduces considerably the intrinsic ill-conditioning of Eq. (3). Even the remaining smaller matrices of the typical dimension 100×100 are still ill-conditioned since a large number of operations lead to inevitable round-off errors. However, with such relatively manageable matrices, this computational noise is more likely to be under control using several specially designed techniques, e.g., singular value decomposition (SVD), Householder's, or Cholesky's decompositions. In DSD we use either SVD or the QZ algorithm as implemented in, e.g., the NAG Library[15] with the successful outcomes. Numerical performance of the DSD algorithm is found do be highly satisfactory from the standpoints of accuracy, stability and robustness. The latter feature, in fact, originates directly from the pre-processing stage, i.e. beamspace windowing, which effectively prepares all the necessary matrix elements $\{U_{nm},S_{nm}\}$ in Eq. (6) by means of the two robust processors, FFT and inverse FFT. We generate the latter two sequences using the appropriate IMSL routine.[16] Overall efficient performance of DSD is comparable with that of FD, since both methods effectively encounter only small size $\sim 100\times 100$ matrices throughout the computation. If required, DSD can spectrally analyze *the whole* Nyquist interval in much the same advantageous fashion as customarily accomplished in FD.

Similar to FD (see Sec. 2 C of Ref. 4), we found that DSD has better resolving power than FFT for the same signal length. Alternatively, the resolution of FFT can be attained by DSD for shorter acquisition time. This is rooted in the uncertainty principles, $N_{\mathrm{FFT}}\propto 2\pi/(\tau\Delta\omega_{\min})$, for FFT and $N_{\mathrm{DSD}}\propto 4\pi/(\tau\Delta\omega_{\mathrm{av}})$, for DSD with $\Delta\omega_{\min}$ and $\Delta\omega_{\mathrm{av}}$ being the minimum and average spacings between eigenvalues in the given window, respectively. As the inequality, $\Delta\omega_{\mathrm{av}}>\Delta\omega_{\min}$, is generally valid, it then necessarily follows that $N_{\mathrm{DSD}}<N_{\mathrm{FFT}}$.

Relative to DSD, which is a parameter estimator, FFT is a spectral estimator, which yields merely the shape of a spectrum. Once a FFT spectrum is available, the peak parameters could be extracted only in a postprocessing stage via nonlinear fitting of each of the resonances to some preassigned forms (Lorentzian, Gaussian, etc). This might be acceptable for well-separated peaks, but it is often unsatisfactory for overlapping resonances. Clearly any nonlinear fitting procedure requires some initial values for the sought pairs $\{\omega_k,d_k\}$ from, e.g., Eq. (3). Since these values are initially unknown, they must be estimated and inadequate guesses could produce significant departures from the true results. As a consequence, the ensuing results often exhibit considerable unphysical and undesirable structures, e.g., ''ripples,'' ''blips'' as well as other oscillations and undulations. Such artifacts are usually noise induced and they might give rise to serious difficulties in the interpretation of the spectral features. It is quite conceivable that this postprocessing in FFT is less useful for dense spectra congested with many lines. These drawbacks of FFT are by and large nonexistent in DSD, which first extracts all the peak parameters $\{\omega_k,d_k\}$ directly *from the time signal* and then constructs the spectrum in the frequency domain using Eq. (7) or Eq. (8).

C. Decimated linear predictor

The DLP is basically comprised of the following three steps: (i) computing the linear prediction coefficients $\{b_k\}$ $(1\leqslant k\leqslant K)$ from the band-limited decimated signal points $\{c_n^{\mathrm{bld}}\}(0\leqslant n\leqslant N_D-1)$, (ii) rooting the DLP polynomial constructed from all the b_k's to obtain the harmonic frequencies ω_k, and (iii) generating the corresponding amplitudes, d_k. With such pairs $\{\omega_k,d_k\}$ at hand, the spectra in any desired mode can be computed from Eq. (7) or Eq. (8).

In order to derive the DLP equations, we begin by writing Eq. (3) in matrix form for the signal points c_{n+1}^{bld} to c_{n+K}^{bld},

$$\begin{pmatrix} c_{n+1}^{\mathrm{bld}} \\ \vdots \\ c_{n+K}^{\mathrm{bld}} \end{pmatrix} = \begin{pmatrix} u_1^{n+1} & \cdots & u_K^{n+1} \\ \vdots & & \vdots \\ u_1^{n+K} & \cdots & u_K^{n+K} \end{pmatrix} \begin{pmatrix} d_1 \\ \vdots \\ d_K \end{pmatrix}, \tag{10}$$

with $u_k=\exp(-i\omega_k\tau_D)$. From the matrix representation Eq. (10) it follows that, for $0\leqslant n\leqslant K$,

$$\begin{aligned} c_n^{\mathrm{bld}} &= (u_1^n\cdots u_K^n) \begin{pmatrix} u_1^{n+1} & \cdots & u_K^{n+1} \\ \vdots & & \vdots \\ u_1^{n+K} & \cdots & u_K^{n+K} \end{pmatrix}^{-1} \begin{pmatrix} c_{n+1}^{\mathrm{bld}} \\ \vdots \\ c_{n+K}^{\mathrm{bld}} \end{pmatrix} \\ &= \sum_{k=1}^{K} b_k c_{n+k}^{\mathrm{bld}}. \end{aligned} \tag{11}$$

In other words, as in the traditional LP method,[10] every signal point c_n^{bld} can be predicted by a linear combination of the others with a fixed set of DLP coefficients $\{b_k\}$ for $1\leqslant k\leqslant K$. The solutions of the system of $K=[(N_D-1)/2]$ linear equations, Eq. (11), give all the unknown DLP coefficients $\{b_k\}$. Using Eq. (3) we can rewrite Eq. (11) as $R_K(u_k)=0$, where the DLP polynomial is given by

$$R_K(u)=\sum_{k=1}^{K} b_k u^k-1, \quad u=e^{-i\omega\tau_D}, \quad u_k=e^{-i\omega_k\tau_D}. \tag{12}$$

The K roots $\{u_k\}$ of the polynomial, $R_K(u)$, provide the frequencies $\{\omega_k\}$ needed for the spectra in Eqs. (7) and (8). Rooting of $R_K(u)$ is a nonlinear operation which implies that both DLP and LP are nonlinear signal processors. The roots of $R_K(u)$ can be found, in principle, by application of, e.g., Laguerre's or Newton–Raphson's method.[17] However, when the polynomial is of high degree $(K\gtrsim 60)$, an alternative method, i.e., diagonalization of the Hessenberg matrix,

$$\mathbf{B}=\begin{pmatrix} -\frac{b_{K-1}}{b_K} & -\frac{b_{K-2}}{b_K} & \cdots & -\frac{b_1}{b_K} & -\frac{b_0}{b_K} \\ 1 & 0 & \cdots & 0 & 0 \\ 0 & 1 & \cdots & 0 & 0 \\ \vdots & & & & \vdots \\ 0 & 0 & \cdots & 1 & 0 \end{pmatrix}, \quad (13)$$

for which the characteristic polynomial $P(z)=\det[\mathbf{B}-u\mathbf{I}]$ coincides with $R_K(u)$ of Eq. (12) with $b_0=-1$, provides a numerically more robust technique for finding the required zeros.[17]

To obtain the remaining unknowns, the amplitudes $\{d_k\}$, DLP uses the computed set $\{\omega_k\}$ to solve the system of K linear equations condensed in Eq. (3). It is well known that the two systems of linear equations contained in Eqs. (3) and (11) are notoriously ill-conditioned. This is the main obstacle for an implementation of the conventional LP which uses the original long signal $\{c_n\}$. However, DLP employs the short band-limited decimated signal $\{c_n^{\mathrm{bld}}\}$ instead of $\{c_n\}$ and ill-conditioning, although still present, is less critical, thus allowing SVD and similar algorithms to be effective in both Eqs (3) and (11).

D. Decimated Padé approximant

For the present purpose of the spectral analysis, it is convenient to introduce DPA using the discretized Fourier integral $F^{\mathrm{bld}}(\omega)$, which is defined at any real frequency ω by the following finite summation:

$$F^{\mathrm{bld}}(\omega)=\sum_{n=0}^{N_D-1} c_n^{\mathrm{bld}}u^{-n}, \quad u=\exp(-i\omega\tau_D) \quad (14)$$

with the same notation as before and where, in particular, the variable u has the same definition as in Eq. (12). The right-hand side of Eq. (14) reduces to the familiar DFT for the values of ω at the Fourier grid, $\omega=2\pi m/T$, $(0\leqslant m\leqslant N_D-1)$. It appears that $F^{\mathrm{bld}}(\omega)$, as an ordinary polynomial, converges slowly with the increasing length N_D of the band-limited decimated signal $\{c_n^{\mathrm{bld}}\}$.

In order to proceed further, let us assume for the moment that the signal points c_n^{bld} are known up to infinity, $0\leqslant n\leqslant\infty$. Recalling that the ultimate goal here is to determine the $2K$ parameters $\{d_k,\omega_k\}$ in Eq. (3), we assume that $N\geqslant 2K$, which is necessary by the algebraic condition requiring, as a minimum, equality between the numbers of equations and unknowns. Then the above-mentioned completion of the given signal $\{c_n\}(0\leqslant n\leqslant N_D-1)$ to the whole interval $n\in[0,\infty]$ is now equivalent to assuming that a solution for the $2K$ parameters can be found such that all $c_n^{\mathrm{bld}}(0\leqslant n\leqslant\infty)$ are either explicitly known or formally given by Eq. (3). Hence we can extend the sum in Eq. (14) to infinity. As such, this algebraically manageable and consistent procedure will yield the way to solve for the numerical values of the searched peak parameters $\{d_k,\omega_k\}$. Interpreting the members of the set $\{c_n^{\mathrm{bld}}\}$ as the coefficients of a Maclaurin series in the variable u^{-1}, we can then define the function $G^{\mathrm{bld}}(u)\equiv F^{\mathrm{bld}}(\omega)=\Sigma_{n=0}^{\infty}c_n^{\mathrm{bld}}u^{-n}$. With Eq. (3) and the sum rule for geometric series we obtain

$$G^{\mathrm{bld}}(u)\equiv\sum_{n=0}^{\infty}c_n^{\mathrm{bld}}u^{-n}=\sum_{k=1}^{K}d_k\sum_{n=0}^{\infty}(u_k/u)^n$$

$$=\sum_{k=1}^{K}\frac{ud_k}{u-u_k}\equiv\frac{P_K(u)}{Q_K(u)}. \quad (15)$$

The right-hand side of Eq. (15) is the so-called *diagonal* decimated Padé approximant given as a rational function with polynomials of degree K in the numerator and denominator. Evidently, the parameters $u_k=\exp(-i\omega_k\tau_D)$ are the poles of $G^{\mathrm{bld}}(u)$, i.e., the zeros of the polynomial $Q_K(u)$.

Of course, the assumption that the coefficients c_n^{bld} are known up to infinity is not fulfilled and, therefore, the sum on the left-hand side of Eq. (15) cannot be evaluated in practice. However, the convergence of the sum can be accelerated by application of DPA. Indeed, with DPA, calculation of the $2K$ coefficients of the two polynomials (note that $p_0=0$),

$$P_K(u)=\sum_{k=1}^{K}p_ku^k, \quad Q_K(u)=\sum_{k=1}^{K}q_ku^k-1, \quad (16)$$

can be achieved provided that a sufficient number of signal points is known, i.e., $N_D>2K$.

At this point, it is important to define the so-called ''current order'' $L\leqslant K$ of the actual DPA, $P_L(u)/Q_L(u)$ as the order of the denominator polynomial, $Q_L(u)$. The adjective ''current'' is used to indicate that DPA can converge at some order L before the actual ''full order'' $K=[(N_D-1)/2]$ in Eq. (16) has been attained. In practice, convergence of DPA is reached at some $L=L_{\max}$ when $P_L(u)/Q_L(u)$ becomes approximately constant with increasing L in the given interval $[L-\Delta L,L+\Delta L]$ of the estimated length ΔL. This concept will prove crucial for devising a new noise reduction technique within the so-called variant (I) defined in Sec. II F.

The unknown coefficients $\{q_k\}$ in Eq. (16) are obtained by equating $G^{\mathrm{bld}}(u)$, which originates from Eq. (14), with the rational fraction of Eq. (15), subsequently multiplying both sides by $Q_K(u)$, and finally comparing the coefficients of the like powers of u. Such a procedure leads to the following system of linear equations:

$$c_n^{\mathrm{bld}}=\sum_{k=1}^{K}q_kc_{n+k}^{\mathrm{bld}} \quad (0\leqslant n\leqslant N_D-1), \quad (17)$$

which can be solved using either SVD or LU decomposition with iterative refinement of the solutions, with the results of the two procedures being the same to within machine accuracy. The coefficients $\{p_k\}$ are then given by the *explicit* formula:

$$p_k=\sum_{n=0}^{K-k}q_{k+n}c_n^{\mathrm{bld}} \quad (1\leqslant k\leqslant K). \quad (18)$$

The zeros $\{u_k\}$ of the denominator polynomial, $Q_K(u)$, give the required complex frequencies,

$$\omega_k=\frac{i}{\tau_D}\ln(u_k). \quad (19)$$

The corresponding amplitudes $\{d_k\}$ are calculated as the residues of the DPA *ansatz*, $P_K(u)/Q_K(u)$. This yields, in the case of distinct zeros $\{u_k\}$, the following result:

$$d_k=\frac{P_K(u_k)}{u_kQ_K'(u_k)}, \quad Q_K'(u)=\frac{dQ_K(u)}{du}. \tag{20}$$

The analytical expression, Eq. (20), in DPA should be contrasted with the corresponding considerable effort invested in DLP and DSD. In DLP the set $\{d_k\}$ is obtained as a numerical solution of the system of linear equations in Eq. (3). In DSD, the values of $\{d_k\}$ necessitate the knowledge of the whole set of eigenvectors $\{B_{nk}\}$ as is clear from Eq. (9).

In the derivation of the DPA method presented here, we have assumed that the signal takes the form given in Eq. (3), i.e., consists of a sum of damped exponentials. However, it is important to note that DPA is not restricted to signals of the form of Eq. (3) as opposed to FD, DSD, and DLP. Indeed, no prior assumptions regarding the nature of the $c_n^{\rm bld}$ need be made in order to solve Eqs. (18) and (17) for the coefficients p_k and q_k, respectively. It is only in the determination of the signal parameters ω_k and d_k that an underlying model for the $c_n^{\rm bld}$ is required.

E. Equivalence of DSD, DLP, and DPA

Comparison between Eqs. (11) and (17) reveals that polynomial $R_K(u)$ from DLP is identical to the denominator polynomial $Q_K(u)$ in DPA:

$$R_K(u)=Q_K(u), \quad \{b_k\}=\{q_k\} \quad (1\leqslant k\leqslant K), \tag{21}$$

with the understanding, $b_0=q_0=-1$. Therefore, DLP and DPA share the common set $\{\omega_k\}(1\leqslant k\leqslant K)$ of the eigenfrequencies. To extend this equivalence to DSD, we rewrite Eq. (11) in the matrix form:

$$c_n^{\rm bld}=\sum_{k=1}^{K} b_kc_{n+k}^{\rm bld}, \quad \mathbf{C}^{\rm bld}=\mathbf{B}'\mathbf{D}$$
$$(0\leqslant n\leqslant K-1,\ 1\leqslant k\leqslant K), \tag{22}$$

where $\mathbf{C}^{\rm bld}$ and $\mathbf{B}'$ are column matrices with the elements $\{c_n^{\rm bld}\}$ and $\{B'\}\equiv\{b_k\}$, whereas $\mathbf{D}$ is the $K\times K$ matrix built from the elements $\{D_{nk}\}\equiv\{c_{n+k}^{\rm bld}\}$. It is apparent that scaling the index k according to, $k=m+1$, in Eq. (22), together with the definition $b_0=-1$ as in Eq. (21), yields the following result:

$$D_{nm}=U_{nm}=c_{n+m+1}^{\rm bld} \quad (0\leqslant n\leqslant K-1,\ 0\leqslant m\leqslant K-1). \tag{23}$$

This proves that the key matrices $\mathbf{D}$ and $\mathbf{U}$ in DLP and DSD, respectively, have the same matrix elements and, therefore, their eigenfrequencies $\{\omega_k\}$ are identical to each other. Hence the equivalence between DLP and DSD. By implication, the same set $\{\omega_k\}(1\leqslant k\leqslant K)$ is shared by DSD, DLP, and DPA. The polynomials $R_K(u)$ and $Q_K(u)$ originate from the secular equation (also known as the characteristic polynomial) of the evolution matrix $\mathbf{U}$. As is well known the eigenvalues of $\mathbf{U}$ coincide with the zeros of the secular equation. *This* is the basis for the equivalence among the present three methods: DSD, DLP, and DPA.

The amplitudes $\{d_k\}$ are obtained in different ways in each of the three methods. The three sets of $\{d_k\}$'s will be the same, provided that the solutions of Eqs. (5), (11), and (17) are unique. Uniqueness is guaranteed when the following two conditions are fulfilled: (i) all the roots $\{u_k\}$ $(1\leqslant k\leqslant K)$ are distinct, i.e., nondegenerate $(u_{k'}\neq u_k$ if $k'\neq k)$ and (ii) the determinants of matrices $\mathbf{U}$ and $\mathbf{S}$ are nonzero. Throughout the present paper, as already mentioned, we restrict our analysis to those signals that are modeled exclusively by Eq. (3). Such a representation with the time-independent amplitudes d_k is only possible for the nondegenerate ω_k's. Nondegeneracy of u_k does not imply nondegeneracy of ω_k due to Eq. (19) with a complex logarithm which has infinitely many branches, i.e., values. Nevertheless, single-valuedness can be secured by selecting, e.g., the principal branch of the complex logarithm so that condition (i) is satisfied. As to condition (ii), the input data $\{c_n\}$ must be such that the restrictions $\det\mathbf{U}\neq 0$ and $\det\mathbf{S}\neq 0$ are met for otherwise the generalized eigenvalue problem in Eq. (5) would be singular precluding the existence of the solutions, as is clear from the Cramer rule. The overall conclusion which clearly emerges from the above-mentioned comparative analysis of the three methods is that DPA is faster and more stable than FD, DSD, and DLP. An enhanced stability of DPA comes from generation of all the $\{d_k\}$'s without any additional effort. By comparison, within, e.g., FD, the set $\{d_k\}$ is computed in a way similar to DSD with a supplementary averaging necessary to reach the required accuracy.

It should be mentioned that, in addition to the genuine frequencies $\{\omega_k\}$, each of the three presented methods find a number of spurious or extraneous resonances. In DSD, we employ an approach used previously with FD[4] whereby such frequencies are identified as those solutions of Eq. (5) that are different for any two chosen powers of the evolution operator $U^p(\tau_D)$, say $p=1$ and $p=-1$. We set a threshold for this difference and reject all frequencies that do not meet the required accuracy. Similar procedures are also implemented in DLP and DPA. In DLP, for example, the mentioned two values $p=\pm 1$ correspond precisely to the forward/backward decimated linear predictions $c_n^{\rm bld}=\sum_{k=1}^{K} b_kc_{n\pm k}^{\rm bld}$, respectively. Likewise, in DPA the first upper/lower paradiagonals, $P_{K\pm 1}(u)/Q_K(u)$, relative to the diagonal decimated Padé approximant are related directly to the two powers $p=\pm 1$ of $U(\tau_D)$, respectively.

F. Noise reduction

Our previous experience in Ref. 6 showed that for experimentally measured signals which are embedded in noise, the above-presented methods find a number of peaks due to noise that, as such, should be removed. To this end, we propose a simple scheme which works quite well in the cases studied so far. It is based upon an enhanced sensitivity of the noise peaks relative to the signal peaks. We detect this sensitivity in two alternative variants: (I) varying the ''current order'' $L\leqslant K$ of DPA from $P_L(u)/Q_L(u)$, and (II) adding some 5%–10% random white noise (zero-mean Gaussian

distributed) to the original time signal $\{c_n\}$, which has already been corrupted with an unspecified level of noise.

This is rationalized by an expectation that random noise possesses widely spread frequencies, nearly a continuum, across the whole spectrum and is, therefore, poorly represented by any mathematical modeling with an isolated resonance approximation, i.e., a single pole *ansatz*, as used both here and in other harmonic inversion signal processing schemes.[3,4,10] Changing these parameters, we search for stable spectral structures that can, in turn, be identified as the true signal peaks. The remaining unstable peaks are viewed as noise that, as such, can be discarded from the final spectra in Eqs. (7) and (8). Here, the practical key problem is to find a parameter which can be changed in a physically and computationally justifiable manner. Clearly, the ultimate goal would be to automate the whole procedure, such that the variation of the chosen parameter itself selects the noise poles to be dropped without the user's intervention. Intuitively, one would expect that a confident tracking of the positions of individual poles should be rather subjective. This is because noise structures generally swing and interchange, precluding the sought correspondence among the poles from successive runs. A more global approach is therefore needed and the above-mentioned two techniques, i.e., variants (I) and (II) will be tested presently for this purpose.

In variant (I) the tracking of the spectral peaks is performed as a function of the signal length N_D of the band-limited decimated signal c_n^{bld}. This is equivalent to varying the size of the Krylov basis set in DSD or to changing the ''current order'' L of the actual DPA, which is $P_L(u)/Q_L(u)$ where $L \leqslant K \equiv [(N_D-1)/2]$. As defined in Sec. II D, the order of DPA is given by the order of its denominator polynomial. Here, gradually increasing the order L is expected to lead to convergence of DPA and this has indeed been confirmed for noiseless signals. On the other hand for ''noisy'' signals the following pattern has been seen to take place systematically. As we progressively increased the order L to a certain value $L_{\max} \leqslant K$, some peaks began to noticeably stabilize their parameters. The other structures did not follow this pattern as they frequently changed their shapes in a nontraceable way and eventually disappeared. This simple procedure seems to be capable of self-selecting the poles to be dropped while using DPA. Equivalently in DSD, an increase of the value of L automatically enlarges the size of the data matrix which represents an upper bound on the dimension of the implied set of the Krylov basis functions utilized to construct the matrices **U** and **S** to be diagonalized.[4] In other words, whenever L increased by a given fraction, the basis size was augmented by the same amount and hence also the total number of poles. Ultimately, the maximal number $L_{\max} \leqslant K$ of Lorentzians in the studied spectrum is *one of the final outcomes* of the spectral analysis within DPA or DSD. By contrast, such a number must be *fixed in advance* in DLP in order to be able to solve Eq. (11) and since it is unknown it ought to be surmised.

In the described procedure, it is intuitively clear that the stable poles would be the first to converge. This is because any of the signal processors for Eq. (3), in fact, represents a fitting of that signal to Lorentzian parameters. In particular in DSD, such a fit is converted to a diagonalization. This diagonalization procedure tries to minimize variances in their variational justification for using, by necessity, incomplete basis sets. They always yield first, as the basis increases, the poles that the basis can model well, i.e., the stable peaks of the true signal. This is reminiscent of resonance scattering in physics, where the stabilization method (SM)[18,19] can discriminate stable poles for the free resonant states from unstable poles for the background as a function of the basis size. Exactly like in SM, the situation in signal processing begins to become unstable again if L is too short or too large. Hence we searched for this region of stability ΔL and the results of variant (I) of SM are presented in Sec. III, Fig. 5. For a cross validation of this procedure, we also check the stability of the peaks in the ΔL region by varying other parameters that should leave the spectrum invariant. Such parameters are, e.g., dropping a given number of the initial signal points of the original signal c_n, changing window size, etc.

As outlined previously, when applied to signal processing, SM consists of searching for the stabilization diagrams or lines that represent the areas of the constancy of the peak parameters when some of the characteristics of the given signal processor are varied. Alternative to the described variant (I), the above-mentioned variant (II) of SM is implemented by adding a sizable 5%–10% random white noise to the already ''noisy'' signal. This is followed by searching for the stable numerical values of the peak parameters. The found stable structures are interpreted as originating from the true signal and, as such, kept in the final spectra. Likewise, the unstable spectral features that could be successfully identified are conceived as being due to noise and the corresponding part of the set $\{\omega_k, d_k\}$ is discarded from Eqs. (7) and (8). Variant (II) of SM is illustrated in Sec. III, Fig. 4.

At first glance, variant (II) might sound rather paradoxical. Nevertheless, such a procedure can be readily justified by the fact that the additional noise is effectively equivalent to a change of the basis functions in DSD or the order of the rational approximation in DPA. Viewed in this way, variants (I) and (II) of SM are, in fact, theoretically equivalent. Of importance is to realize that, once we conceive DSD as a basis set method, we are entitled to *change the basis functions* and thus to manipulate the noise in order to disentangle it from the genuine signal. This latter goal can similarly be setup and ultimately achieved within DPA by *changing the order of a rational approximation* which models the true spectrum.

III. EXAMPLES

Here we present the results of our computations related to both the diagonalization and signal processing applications of DSD, DLP, and DPA. The diagonalization aspect is addressed first and for this purpose we present the eigenvalues of the Hamiltonian of SO_2 calculated using the corresponding time autocorrelation functions.[2] In this particular case, the time autocorrelation functions are both real and time symmetric, i.e., $c_{-n} = c_n (0 \leqslant n \leqslant N-1)$. In FD,[4] such a symmetry is exploited advantageously to construct a real symmetric analog of the generalized eigenvalue problem, Eq.

TABLE I. Comparison between calculated energies in cm^{-1} for local mode doublets of SO_2. Calculations: DSD (decimated signal diagonalization), DLP (decimated linear predictor), DPA (decimated Padé approximant), and FD (filter diagonalization—Ref. 2). Calculated energies were obtained using $N=180\,000$ values of the autocorrelation function c_n generated by the Chebyshev wave packet propagation method and kindly provided to us by H. Guo—Ref. 2). The labels n_1, n_2, and n_3 denote the quantum numbers for symmetric stretch, bend and antisymmetric stretch, respectively.

n_1	n_2	n_3	Parity	DSD	DLP	DPA	FD
9	0	0	Even	10 102.408 08	10 102.408 08	10 102.408 08	10 102.41
8	0	1	Odd	10 252.159 32	10 252.159 32	10 252.159 32	10 252.16
10	0	0	Even	11 188.293 52	11 188.293 52	11 188.293 52	11 188.29
9	0	1	Odd	11 327.148 54	11 327.148 54	11 327.148 54	11 327.15
11	0	0	Even	12 266.732 73	12 266.732 73	12 266.732 73	12 266.73
10	0	1	Odd	12 395.303 73	12 395.303 73	12 395.303 73	12 395.30
12	0	0	Even	13 337.637 69	13 337.637 69	13 337.637 69	13 337.64
11	0	1	Odd	13 455.264 91	13 455.264 91	13 455.264 91	13 455.26
13	0	0	Even	14 400.874 30	14 400.874 30	14 400.874 30	14 400.87
12	0	1	Odd	14 506.834 55	14 506.834 55	14 506.834 55	14 506.83
14	0	0	Even	15 456.271 20	15 456.271 20	15 456.271 20	15 456.27
13	0	1	Odd	15 549.760 11	15 549.760 11	15 549.760 11	15 549.76
15	0	0	Even	16 503.491 36	16 503.491 36	16 503.491 36	16 503.49
14	0	1	Odd	16 583.681 06	16 583.681 06	16 583.681 06	16 583.68
16	0	0	Even	17 542.063 13	17 542.063 13	17 542.063 13	17 542.06
15	0	1	Odd	17 608.158 00	17 608.158 00	17 608.158 00	17 608.16
17	0	0	Even	18 571.174 53	18 571.174 53	18 571.174 53	18 571.17
16	0	1	Odd	18 622.483 04	18 622.483 04	18 622.483 04	18 622.48
18	0	0	Even	19 589.491 27[a]	19 589.491 27	19 589.491 27	19 589.49
17	0	1	Odd	19 626.618 20	19 626.618 20	19 626.618 20	19 626.62
19	0	0	Even	20 594.888 52	20 594.888 52	20 594.888 52	20 594.89
18	0	1	Odd	20 618.595 71	20 618.595 71	20 618.595 71	20 618.60
20	0	0	Even	21 584.788 43	21 584.788 43	21 584.788 43	21 584.79
19	0	1	Odd	21 597.974 32	21 597.974 32	21 597.974 32	21 597.97
21	0	0	Even	22 557.234 51	22 557.234 51	22 557.234 51	22 557.23
20	0	1	Odd	22 564.314 40	22 564.314 40	22 564.314 40	22 564.31
22	0	0	Even	23 511.932 46	23 511.932 46	23 511.932 46	23 511.93
21	0	1	Odd	23 514.839 59	23 514.839 59	23 514.839 59	23 514.84
23	0	0	Even	24 449.460 58	24 449.460 58	24 449.460 58	24 449.47
22	0	1	Odd	24 450.941 35	24 450.941 35	24 450.941 35	24 450.94

[a]The DSD result for level (18,0,0) was reported incorrectly in Ref. 1.

(5). In DSD, for example, the situation is somewhat different, since the band-limiting process is not time invariant so that generally complex values for the $\{c_n^{\mathrm{bld}}\}$'s are obtained. As a result, the associated matrix elements in Eq. (5) are also complex. However, this apparent drawback turns out to be insignificant in practice. This is because we always encounter only small size matrices and the additional computational effort required to solve Eq. (5) with complex arithmetic remains negligible relative to the calculation of the time autocorrelation functions themselves. Note, however, that the accurate results for all of the energies presented in Table I can only be obtained by using the ''negative time'' information from the values of $\{c_n\}$'s. In principle, this can be accomplished efficiently either by including all $2N-1$ of these $\{c_n\}$'s in the construction of the low-resolution spectrum by the standard FFT or alternatively by replacing this step with a fast cosine Fourier transform. This latter option, however, cannot be combined with the *inverse* FFT employed to compute the band-limited signal c_n^{bld} from the windowed low-resolution spectrum. Previously in Ref. 1 we compared the energies of the local mode doublets of SO_2 below $25\,000\,cm^{-1}$ calculated with DSD with the corresponding results obtained using FD.[2] Table I extends this comparison to include the corresponding energies obtained with DLP and DPA. We see that DSD, DLP, and DPA are in perfect mutual agreement, as expected from the equivalence of these three methods proven in Sec. II E. Moreover these three methods reproduce the results of FD almost exactly and the only exception here is a small difference of $0.01\,cm^{-1}$ for level (23,0,0).

Next we display and discuss the results obtained for the performed tests of DSD/DLP/DPA methods in both the case of theoretically synthesized model signals of the form given in Eq. (3) with the known complex peak parameters $\{\omega_k, d_k\}$ and the case of experimentally measured ICR as well as NMR data. We systematically compared the present three techniques with each other and found that they always give identical results to within machine accuracy as expected from Sec. II E. Hence it suffices that in the rest of this section with the illustrations we refer only to one of them, e.g., DPA.

First, noiseless spectra obtained by applying FFT and DPA to a simulated time signal of the form of Eq. (3) taken from Ref. 7 are shown in Fig. 2. An inspection of Fig. 2 reveals two obvious differences between DPA and FFT

(i) The DPA resolves the doublet at 0.505–0.510 kHz, which is missed in FFT. The intrinsic resolution of FFT, i.e., $2\pi/T$, would permit detection of this doublet for the chosen signal length $N=512=0.5\,K$, but the widths are too broad to separate the two peaks from each other.

(ii) Some of the peak heights calculated by FFT are ac-

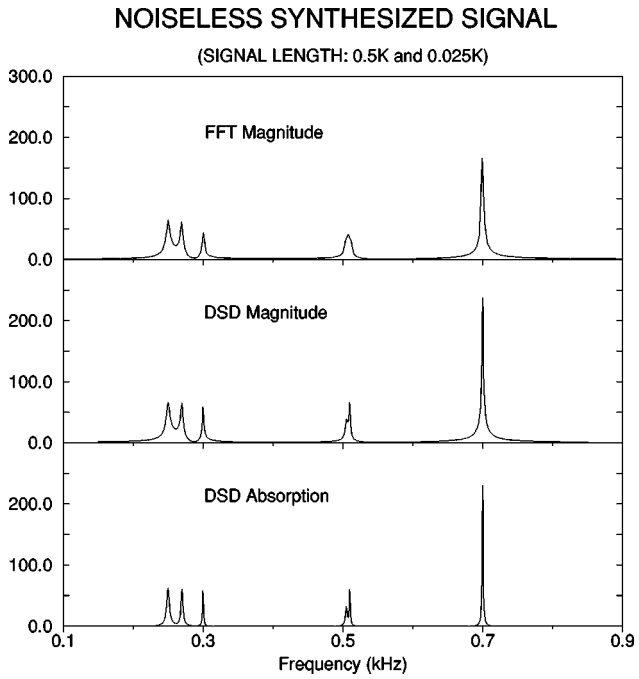

FIG. 2. Spectra for a noiseless synthesized time signal consisting of the sum of six exponentially damped sinusoids with the known amplitudes, phases, and damping constants taken from Ref. 7. DSD magnitude and absorption spectra are shown in Figs. 2 and 3. DPA and DLP give the same results.

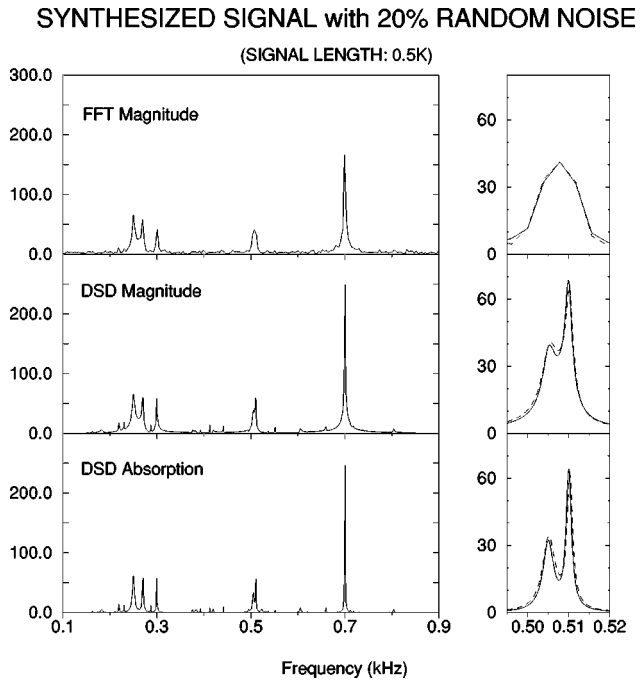

FIG. 3. Spectra for a ''noisy'' synthesized time signal consisting of the sum of six exponentially damped sinusoids with the known amplitudes, phases, and damping constants taken from Ref. 7. The Gaussian distributed zero-mean random noise of standard deviation 20 is added to the signal. The panels in the right-hand column show magnifications of the doublet at 0.505–0.510 kHz with the full and dashed lines representing the noiseless and ''noisy'' spectra, respectively.

curate only when using the full signal length of $N=512$, whereas those obtained with DPA are exactly those of the input parameters, even at $\sim N/20=0.025\,\mathrm{K}$.

In the second example, a time signal was constructed identical to the one used for Fig. 2, except that Gaussian distributed white noise with zero-mean and standard deviation $\sigma=20$ is added. This 20% noise contamination of the signal produces FFT and DPA spectra that are depicted in Fig. 3. The superior frequency resolving power of DPA is clear and, in contrast to FFT, the present method again separates the close doublet at 0.505–0.510 kHz, which is further magnified in the panels on the right-hand side of Fig. 3. The spectra calculated by DPA have not been subjected to any noise reduction procedures, and yet the successful resolution of all six genuine peaks is achieved without any difficulty.

In the third example we study a problem of noise reduction and illustrate the utility of the stabilization method (SM).[18,19] For this purpose, we again use the synthesized signal with 20% noise from the second example. Here, rather than using model-dependent parameters to detect the stable poles, we employ a ''generic-type feature'' consisting of adding more noise to the already ''noisy'' signal. This provides an illustration of variant (II) from Sec. II F.

Basically, we add an additional 7.5% Gaussian distributed, zero-mean white noise on top of the existing 20% noise level, compute the peak parameters, and repeat the same procedure, each time starting with the original signal. In so doing we do not introduce progressively more noise, but rather each time a different 7.5% ''noisy'' distribution is added to the original signal. Each repeated DPA calculation results in a new set of peak parameters, $\{\omega_k,d_k\}$. The parameters found from this sequence of calculations could be averaged over in order to produce a somewhat cleaner final spectrum. However, we find that plotting the peak positions found in each calculation is far more illuminating.

The absorption spectra depicted in the top panels of Fig. 4 are obtained by the straightforward direct runs of DPA for the two selected windows, $\omega\in[0.2,0.35]\,\mathrm{kHz}$ and $\omega\in[0.45,0.55]\,\mathrm{kHz}$, in which we know that we have three and two signal peaks, respectively. The lower panels represent the variation of $\mathrm{Re}(\omega_k)$ as a function of frequency, ω, for each of 50 different DPA calculations displayed as crosses at the ordinate axis. As seen in the lower panels of Fig. 4, for some of the peaks $\mathrm{Re}(\omega_k)$ exhibits an extraordinary stability along the ordinate and, as such, they appear insensitive to the presence of the additional 7.5% level of noise. Other structures, however, appear to be more unstable. The former are recognized to be the known true peaks, whereas the latter ones are identified as noise and can be dropped from the ''line list'' $\{\omega_k,d_k\}$ to obtain a cleaner spectrum. A closer inspection of the peak parameters obtained from each different DPA calculation reveals that those of the true signal are identical to several significant figures, whereas those of the corresponding noise poles are more widely dispersed. Indeed SM appears to work spectacularly well for this synthesized signal and it is a straightforward task to distinguish between noise and signal features. This, as an illustration of the variant (II) from Sec. II F, provides evidence that SM can be used successfully in noise identification for signal processing.

Next we present in Fig. 5 the results of our fourth example concerning a protein isotopic fine structure. The ex-

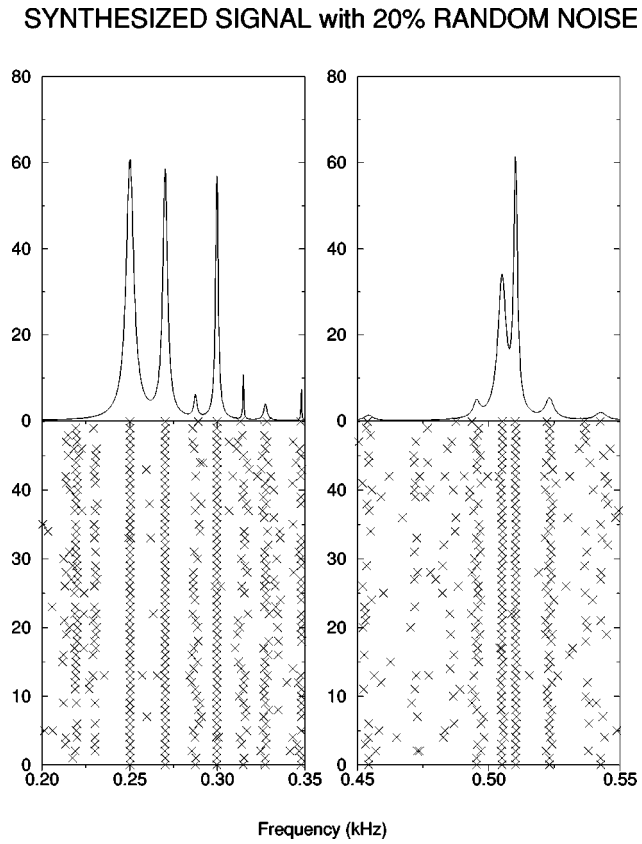

FIG. 4. Absorption spectra for a ''noisy'' synthesized time signal consisting of the sum of three (left) and two (right) exponentially damped sinusoids with the known amplitudes, phases, and damping constants taken from Ref. 7. The Gaussian distributed zero-mean random noise of standard deviation 20 is added to the signal. Top panel: The straightforward direct runs of DPA. Bottom panel: Variant (II) of the stabilization method with an additional 7.5% random white noise on top of the already existing 20% noise (see the text). The crosses represent $\mathrm{Re}(\omega_k)$ obtained from 50 different DPA calculations that are the ordinates.

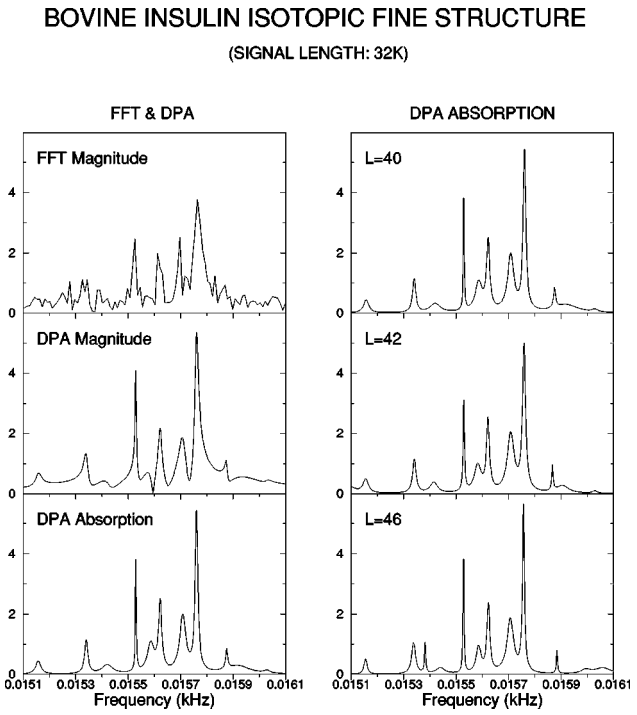

FIG. 5. ICR spectra of bovine insulin. Chirped excitation. Signal supplied by A. Marshall, NHMFL-FSU (Ref. 20) and obtained through a single time-domain data acquisition by means of the external accumulation electrospray ionization (ESI) together with the heterodyne quadrature (Ref. 20). The number L given in each panel in the right column is the ''current order'' of DPA (see the text).

perimental ICR time signal for bovine insulin was obtained by means of the external accumulation electrospray ionization (ESI) at NHMFL (Tallahassee).[20] The measured time signal contains a considerable level of noise as is clear from the FFT spectrum. Here, we illustrate the variant (I) for noise identification as described in Sec. II F. We empirically determine the converged order L of DPA, which leads to rather stable spectral features as is evident from the right-hand side of Fig. 5. As can be seen in Fig. 5, the FFT has difficulty in unambiguously resolving some peaks even with the full signal length, $N=32\,\mathrm{K}$. Also from Fig. 5, however, it is obvious that DPA is distinctly more successful than FFT, since it can resolve all the individual elemental compositions with their correct relative abundances.[20] We know this as the pattern of peaks and their relative heights seen in the present DPA magnitude spectrum is in remarkably good agreement with a simulated Monte Carlo spectrum which has been reported previously in Ref. 20 (not shown in Fig. 5 to avoid clutter).

Our fifth example is the experimental ICR time signal for equine myoglobin and bovine carbonic anhydrase II that have been recorded using ESI at NHMFL (Tallahassee).[20] The results for FFT and DPA spectra are depicted in Fig. 6.

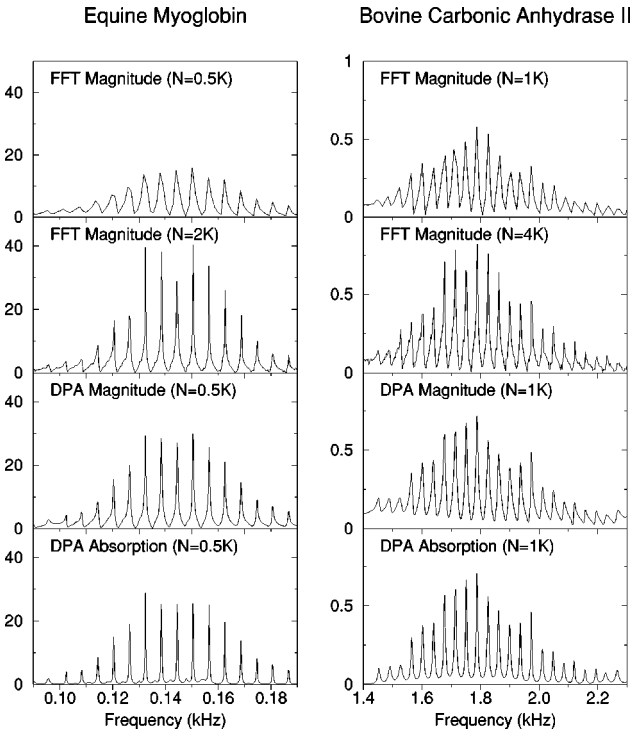

FIG. 6. ICR spectra of equine myoglobin (left) and bovine carbonic anhydrase II (right). Pulsed excitation. Both signals of length $N=8$ K were supplied by A. Marshall, NHMFL-FSU (Ref. 20) and obtained through a single time-domain data acquisition by means of the external accumulation electrospray ionization (ESI) together with the heterodyne quadrature (Ref. 20).

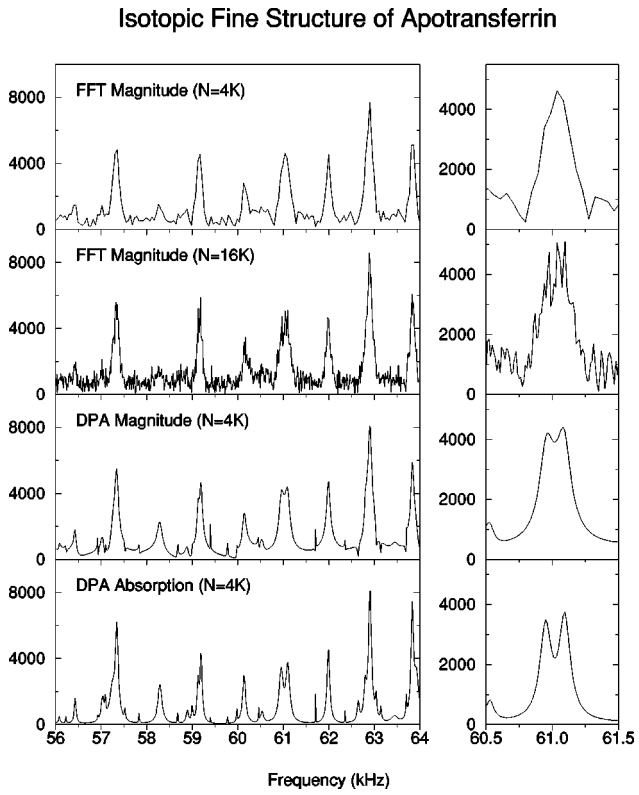

FIG. 7. ICR frequency spectra of the isotopic fine structure of apotransferrin. The signal was recorded at the Ångström Laboratory (Uppsala, Sweden) (Ref. 21). The panels in the right-hand column show magnifications of the spectra in the region of a doublet located at 61 kHz. The top two panels show the FFT magnitude spectra obtained using $N=4$ K and $N=16$ K of the measured signal points. The bottom panel depicts the corresponding DPA absorption spectrum obtained using $N=4$ K.

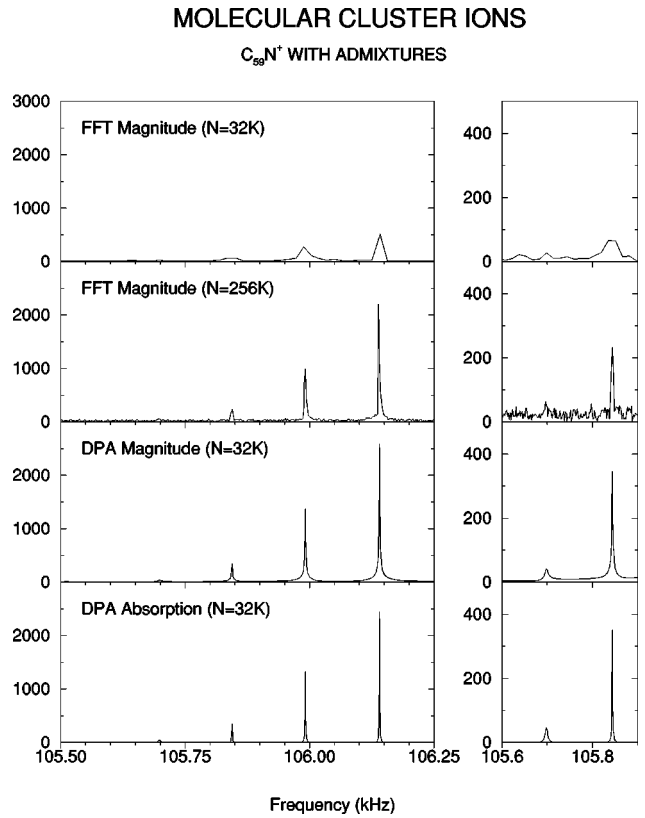

FIG. 8. ICR frequency spectra of singly charged molecular ions $[C_{59}N]^+$ and $[C_{60}]^+$. The time signal was obtained via a single time-domain data acquisition using the matrix assisted laser desorption ionization (MALDI). Using merely one quarter of the full signal length, DPA obtains the entire elemental structure with the correct relative abundance of all the isotopes. The largest peak in the spectrum is associated with the monoisotopic $[^{12}C_{59}{}^{14}N]^+$ ion. The right-hand column shows magnifications of the two smallest peaks.

It is clear from Fig. 6 that DPA is again superior to FFT. In this case, both time signals have rather good signal-to-noise ratios (SNR) and a further noise reduction is unnecessary. Note that the experimental conditions in recording these time signals were such that all the peak widths, as predetermined, should come out to be approximately the same. Indeed this is verified to a satisfactory degree of accuracy in our calculated spectra as seen in Fig. 6.

The sixth example is concerned with the isotopic fine structure of apotransferrin. This experimental ICR time signal was measured at the Ångström Laboratory of the University of Uppsala (Sweden). In this measurement, the standard FFT-ICR method is used together with an accompanying technique called the collisionally induced dissociation.[21] The apotransferrin molecule is rather heavy with mass close to ~ 77 kDa. The sample was electrosprayed in a 50:50 methanol/water mixture to which 2% (vol/vol) acetic acid was added.[21] In Fig. 7 we display the computed FFT and DPA spectra together with a magnification of a small frequency range near a doublet at 61 kHz. With signal lengths of $N=4$ K and $N=8$ K (not shown), FFT is unable to resolve the doublet. *Moreover, the expected increase in FFT resolution is not obtained when further increasing the signal length to* $N=16$ K. This is presumably due to the fact that increasing the acquisition time to attain the necessary resolution has significantly worsened the SNR. Such an occurrence in recording the time signal leads to a considerable deterioration in quality of the resulting FFT spectra. On the other hand, the superior frequency resolving power of DPA is preserved here, thus enabling the separation of the doublet with $N=4$ K signal points as can be seen in the bottom panel of Fig. 7. This example with an excessively ''noisy'' experimental signal is particularly important as it clearly demonstrates the capability of DPA to extract information which is otherwise inaccessible to FFT.

The seventh example is focused on the experimental ICR time signals for $[C_{59}N]^+$ and $[C_{60}]^+$ and the associated spectra calculated by FFT and DPA. These signals were recorded at Department of Chemistry, University of California Santa Barbara (Santa Barbara, CA) by the matrix assisted laser desorption ionization of admixtures of azafullerene, $(C_{59}N)_2$, and fullerene, C_{60}.[8] The corresponding spectra are displayed in Fig. 8 in order of increasing improvement. It is seen in Fig. 8 that to resolve all of the peaks satisfactorily, FFT needs the full signal length of $N=256$ K. On the other hand, DPA arrives at the same result by employing only $N=32$ K. Even with such a signal, which is *eight times* shorter than the one provided with the full acquisition time, DPA resolves the isotopic admixtures to within a fraction of one Da, given the appropriate conversion from the frequency to mass scale.

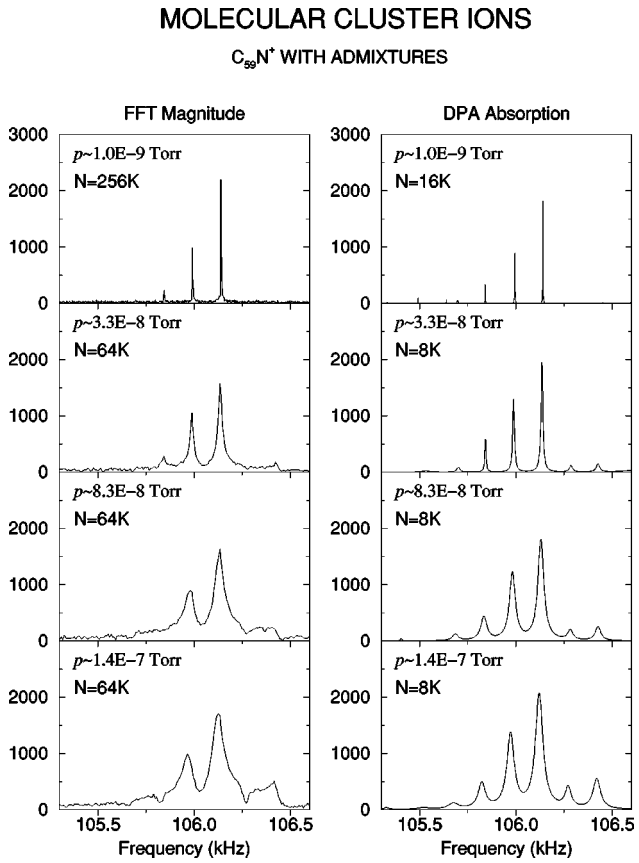

FIG. 9. ICR frequency spectra of singly charged molecular ions $[C_{59}N]^+$ and $[C_{60}]^+$ embedded in the background of argon at different pressures ranging from $p\sim1.0\times10^{-9}$ Torr to $p\sim1.4\times10^{-7}$ Torr. The time signal was obtained via a single time-domain data acquisition using the matrix assisted laser desorption ionization (MALDI). Left and right columns represent FFT and DPA, respectively. Using only a small fraction (1/8–1/16) of the full signal length, DPA obtains all the peak parameters and, in particular, their correct relative heights that are proportional to the relative abundance of the isotopes.

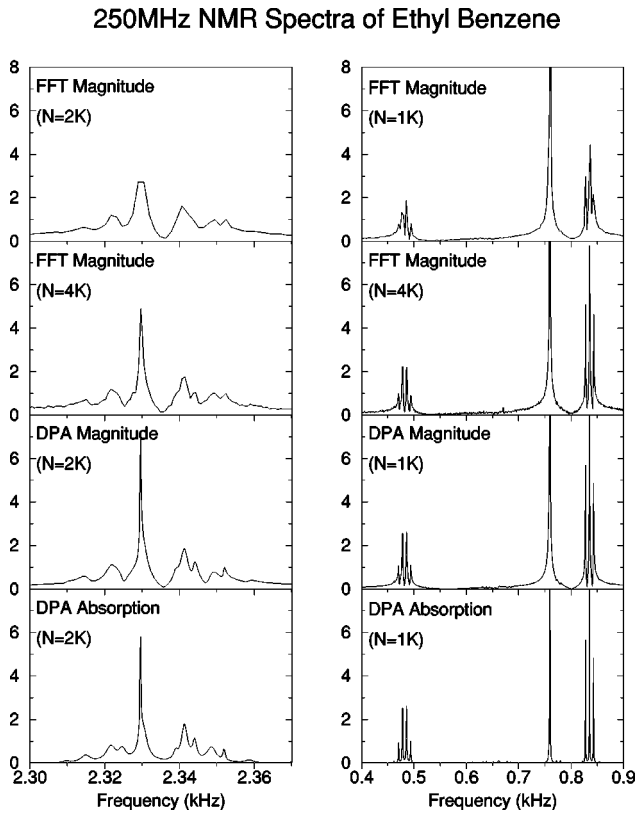

FIG. 10. NMR frequency spectra for a commercial standard 0.1% concentrate of ethyl benzene in $CDCl_3$ solvent. The signal was recorded on a Bruker AC250 NMR Spectrometer. In the right-hand column, the top two panels show the FFT magnitude spectra obtained using $N=1$ K and $N=4$ K of the measured signal points. The bottom two panels display the corresponding DPA magnitude and absorption spectra obtained using $N=1$ K. The left-hand column shows the corresponding spectra for the more complex aromatic region. In this case DPA needs $N=2$ K to reproduce accurately all of the features observed in the FFT magnitude spectrum obtained using the full $N=4$ K of the measured signal points.

Our eighth example shown in Fig. 9 is an extension of the preceding case to the ICR time signal for $[C_{59}N]^+$ which is now embedded in a background of argon at different pressures ranging from $p\sim1.0\times10^{-9}$ Torr to $p\sim1.4\times10^{-7}$ Torr. The signal used in Fig. 8 corresponds to the case $p\sim1.0\times10^{-9}$ Torr, which is nearly equivalent to the situation where the argon buffer is absent during the measurement. As is clear from Fig. 9, DPA significantly outperforms FFT in the resolution power by using only 8–16 times shorter signal lengths at all argon pressures displayed.

All of the above-mentioned examples, including the model problem, fall into a category which is typical for most of the ICR time signals. However, this category does not exhaust the type of signals to which DSD/DLP/DPA methods could be successfully applied. To illustrate this point, we shall now consider the ninth test as our final example using a NMR time signal for a commercial standard 0.1% concentrate sample of ethyl benzene in D-chloroform ($CDCl_3$) solvent. This signal was recorded on a Bruker AC250 NMR Spectrometer at the Department of Chemistry, University of Southern California, (Los Angeles, CA).[22] The corresponding FFT and DPA spectra are depicted in Fig. 10. Again DPA exhibits a better resolving power than FFT. Moreover, DPA achieves higher quality spectra than FFT with considerably shorter lengths of this NMR time signal.

For NMR experiments, the total acquisition time of a single scan is not the time-limiting factor and the required resolution is readily attained with FFT. However, to improve the SNR, it is customary to average the results obtained from perhaps several thousand separate measurements. By working with a shorter signal, which usually invokes less noise, DPA is able to achieve the same result as FFT but with a signal generated from *far fewer* separate measurements. Hence, use of DPA will result in a significant decrease in the time needed to perform the experiments.

We reemphasize here that our previous experience with the stabilization method in resonance quasibound states of atomic and molecular systems helped us to reduce significantly the noise level in realistic experimental signals. The DPA performs excellently in the sense of converging fast and *first* those poles $\{\omega_k\}$ that are close to the unit circle. For such poles the DPA represents a remarkably stable procedure. The reason for this is that these poles are near the real axis and represent localized wave packets comprised of only a limited number of continuum states (noise background)

which can be sufficiently well described either by a locally compact Krylov basis set (DSD) or by a rational approximation (DPA). However, the poles far from the imaginary axis ought to collect a great deal of continuum ''noisy'' states with considerable spreading and, therefore, will not be represented adequately by any of our methods. Here we make a plausible correspondence between resonances, i.e., quasibound states and true signal poles, on the one hand, as well as between continuum states or broad resonances and noise poles, on the other hand.

In these ''continuumlike'' noise poles, some variations of the global parameters such as decreasing the signal length N_D or increasing the noise level in the given frequency window $[\omega_{\min},\omega_{\max}]$ would *de facto* change, e.g., the basis in DSD and introduce greater instabilities. This is a clear *signature* of noise which can afterwards readily be rejected from the spectra in Eqs. (7) and (8). The results of a more detailed study devoted to the noise reduction problem will be reported shortly elsewhere.[23]

Finally, let us consider what happens in decimated harmonic inversion analysis when the noise removal is ''less than perfect'' and contrast it with what occurs when the FFT is used. Figure 7 is useful for this comparison despite the fact that here we actually find it unnecessary to apply our noise reduction procedures to the DPA spectrum. The second row of Fig. 7 shows features typical of the FFT spectrum when a significant level of noise is present. There is an increase in the baseline with excessive oscillations in the spectrum and a considerable loss of resolution caused by noise features ''filling in'' between the existing peaks. The corresponding DPA absorption spectrum prior to noise reduction is displayed in the bottom row of Fig. 7. The DPA spectrum still shows FFT-type oscillations but these are now concentrated into a modest number of usually small peaks; improved resolution is the good news. The noise reduction techniques proposed in this paper could reorganize many of these peaks and hopefully categorize them as noise (see, e.g., Fig. 4).

In situations where the level of noise relative to signal is more significant some noise peaks may remain. Unfortunately, no reliable method yet exists to determine which of the remaining small peaks are signal and which are due to noise. In many ways the ethos of scientific reporting tends to favor and accept the FFT features as ''unavoidable'' but condemns any method that gives ''fake peaks.'' Hence prudence is called for when dealing with the issue of ''small peaks'' such as those found by DPA and displayed, e.g., in the bottom panel of Fig. 3. In a situation with no foreknowledge to lend assurance to an assignment one must simply report the objective uncertainty of the analysis.

Of course, it could happen that a signal is swamped with noise. In such a circumstance our methods will fail as no region showing stable and unstable features will be found. Here the true positions of the peaks are determined by both signal and noise. Obviously the FFT yields equally disastrous outcomes when faced with such situations. In summary, it should be pointed out that the noise reduction methods proposed in Sec. II F are still very much under development and a further thorough study aimed at demonstrating their full range of usefulness and practicality is needed.[23]

IV. CONCLUSION

Three new operationally different but mathematically equivalent, stable user-friendly and robust signal processing methods named decimated signal diagonalization (DSD), decimated linear predictor (DLP), and decimated Padé approximant (DPA) are introduced. They are presently implemented for performing the spectral analysis on experimental data for ion cyclotron resonance (ICR) spectroscopy and nuclear magnetic resonance (NMR) spectroscopy. These parameter estimators are shown to possess several important advantages over the fast Fourier transform (FFT), which is a spectral estimator.

In contrast to the most frequently used signal processor, FFT, which can provide only the shape of a spectrum, DSD/DLP/DPA first determine all the peak parameters (positions, magnitudes, relaxation times, phases, etc.) and then construct a spectrum in any of the desired modes (complex, magnitude, power, absorption). Absorption spectra provide a better resolution than the other modes. The availability of the peak parameters in our methods enables an easy phase correction of the examined complex mode spectrum whenever a certain number of the signal points should be dropped for the reason of the experimental limitations. This ability to phase correct the spectra *de facto* implies that the well-known ''phase problem'' which has plagued ICR and NMR fields for many years no longer exists. To actually generate the absorption spectra, the three proposed methods do not need any additional experimental work or postprocessing as opposed to FFT.

Moreover, our experience in numerous examples, a small part of which is illustrated in the present paper, strongly indicates that the suggested methods are capable of providing highly satisfactory results for a large variety of signals embedded in noise provided caution is exercised as explained in Sec. IV. Excellent quality of the corresponding spectra is achieved using a novel noise reduction technique based upon the stabilization method from the resonance scattering theory. The evidence is presented justifying the usage of an acquisition time which is considerably shorter, by a factor of the order $\sim(8-16)$, than the one customarily used in FFT to arrive at the required resolving power.

The net conclusion which emerges from our analysis indicates that experimental ICR and NMR ''noisy'' time signals might actually contain more information than can be extracted by FFT in the frequency domain. Such a drawback can be overcome by using, e.g., our three parameter estimators, DSD/DLP/DPA. Of these three, DPA is recommended as the optimal method of choice since it requires the least numerical effort to arrive at the best possible result with the optimal signal-to-noise ratio.

ACKNOWLEDGMENTS

The DOE (Contract No. 53-4815-248), the National Science Foundation (NSF Grant No. PHY-9802534), the Donors of the Petroleum Research Fund administered by the

American Chemical Society, the Deutsche Forschungsgemeinschaft, and the Deutscher Akademischer Austauschdienst are each acknowledged for partial support of the present research. J. M. thanks H. S. Taylor and the University of Southern California for their kind hospitality during the initial stage of this work. The authors thank Professor V. A. Mandelshtam for useful discussions as well as the following experimentalists for providing their ICR or NMR signals: Professor A. G. Marshall for bovine insulin, equine myoglobin, and carbonic anhydrase II, Dr. J. Axelsson and MSci. M. Palmblad for apotransferrin, Professor S. K. Shin for carbonic nitrogen and A. Kershaw for ethyl benzene. Professor H. Guo is thanked for supplying his signal for SO_2 together with the associated energy levels computed by means of FD. Dž. Belkić acknowledges partial support from FOUU at the Karolinska Hospital, Stockholm, Sweden.

[1] Dž. Belkić, P. A. Dando, H. S. Taylor, and J. Main, Chem. Phys. Lett. **315**, 135 (1999).
[2] H. Guo (private communication); G. Ma and H. Guo, J. Chem. Phys. **111**, 4032 (1999).
[3] M. R. Wall and D. Neuhauser, J. Chem. Phys. **102**, 8011 (1995).
[4] V. A. Mandelshtam and H. S. Taylor, J. Chem. Phys. **107**, 6756 (1997); **109**, 4128 (1998) (erratum).
[5] J. Main, P. A. Dando, Dž. Belkić, and H. S. Taylor, J. Phys. A **33**, 1247 (2000).
[6] Dž. Belkić, P. A. Dando, J. Main, and H. S. Taylor, J. Phys. Chem. A (submitted).
[7] S. Guan and A. G. Marshall, Anal. Chem. **69**, 1156 (1997).
[8] S.K. Shin and S.-J. Han, Int. J. Mass Spectrom. Ion Processes **153**, 87 (1996); J. Am. Soc. Mass Spectrom. **8**, 86 (1997); S.K. Shin (private communication).
[9] S. D. Silverstein and M. D. Zoltowski, Digital Signal Processing **1**, 161 (1991).
[10] S. L. Marple, Jr., *Digital Spectral Analysis with Applications* (Prentice–Hall, Englewood Cliffs, NJ, 1987).
[11] G. A. Baker, *Essentials of Padé Approximants* (Academic, New York, 1975).
[12] E. J. Weniger, Comput. Phys. Rep. **10**, 189 (1989).
[13] J. Main, P. A. Dando, Dž. Belkić, and H. S. Taylor, Europhys. Lett. **48**, 250 (1999).
[14] Dž. Belkić, J. Phys. A **22**, 3003 (1989).
[15] NAG FORTRAN Library, *Numerical Algorithms Group*, 256 Banbury Road, Oxford OX2 7DE, UK.
[16] IMSL Math/Library Users Manuel, *International Mathematical Statistical Library*, IMSL Inc., 2500 CityWest Boulevard, Houston TX 77042.
[17] W. H. Press, S. A. Teukolsky, W. T. Vetterling, and B. P. Flannery, *Numerical Recipes*, 2nd ed. (Cambridge University Press, Cambridge, 1992).
[18] A. Hazi and H. S. Taylor, Phys. Rev. A **1**, 1109 (1970).
[19] V. A. Mandelshtam, T. R. Ravuri, and H. S. Taylor, J. Chem. Phys. **101**, 8792 (1994).
[20] S. D.-H. Shi, C. L. Hendrikson, and A. G. Marshall, Proc. Natl. Acad. Sci. USA **95**, 11532 (1998).
[21] M. Palmblad, H. Önnerud, K. Håkansson, and J. Axelsson, International Conference of the American Society of Mass Spectrometry, Dallas, TX, 1998); Session CD.
[22] A. Kershaw (private communication).
[23] P. A. Dando, Dž. Belkić, J. Main, and H. S. Taylor (unpublished).